Supplement of Earth Surf. Dynam., 9, 1363–1380, 2021
https://doi.org/10.5194/esurf-9-1363-2021-supplement

Earth Surface Dynamics
Open Access
EGU

Supplement of

Relationship between meteoric ^{10}Be and NO_3^- concentrations in soils along Shackleton Glacier, Antarctica

Melisa A. Diaz et al.

Correspondence to: Melisa A. Diaz (mdiaz@whoi.edu)

Supplement

S1. Exposure age model

We used Eq. 4 from the main text (written again below) to attempt two exposure age proxy estimations: 1) using the measured ^{10}Be inventories for Roberts Massif, Bennett Platform, and Thanksgiving Valley, and 2) by calculating ^{10}Be concentrations using regressions of NO_3^- and ^{10}Be (Fig. S1) for all seven locations with depth profiles.

$$t = -\frac{1}{\lambda} \cdot \ln\left[1 - \frac{\lambda I}{Q - E\rho N}\right] \quad (4)$$

For Eq. 4, t (yrs) represents time since exposure, λ (yr^{-1}) represents the disintegration constant for ^{10}Be radioactive decay, I (atoms cm^{-2}) represents the ^{10}Be inventory, Q (atoms cm^{-2} yr^{-1}) represents the ^{10}Be flux, E (cm yr^{-1}) represents erosion, ρ (g cm^{-3}) is soil density, and N (atoms g^{-1}) is the concentration of ^{10}Be at the surface.

S1.1. Model variable selection and key assumptions

The exposure age calculations are dependent on the selected values for the variables in Eq. 4. We chose a flux value (Q) of 1.3 x 10^5 atoms cm^{-2} yr^{-1} from Taylor Dome (Steig et al., 1995) due to a similar climate to that of the CTAM and an absence of local meteoric ^{10}Be flux data. Soil density (ρ) across the Shackleton Glacier region was approximately 2 g cm^{-3}. We chose a conservative erosion value of 5 cm Ma^{-1} for our analysis of the Shackleton Glacier region.

It is important to note two key assumptions in our variable selection and model development. First, we have assumed a uniform erosion rate across the region. Given the variety of surface features at each location (Table 2), some locations on valley floors, for example, may have increased surface concentrations of meteoric ^{10}Be due to entrapment of fine-grained wind-blown

sediments. Locations on hillslopes and valley walls might have higher erosion rates (Morgan et al., 2010; Schiller et al., 2009). We assumed that deflation of fine-grained material had occurred rapidly on the flat surfaces we sampled due to strong winds over the poorly consolidated tills following soil exposure (Lancaster et al., 2010). Due to a deficit of soil erosion data in the CTAM, we calculated exposure ages (Eq. 4) with the 5 cm Ma^{-1} erosion value and without the erosion/deposition term (E=0). Second, we attempted to estimate the background concentrations and initial inventory for each sample collected furthest from the glacier. We hypothesized that these samples were potentially exposed throughout at least the LGM and had negligible inheritance, though this was merely an assumption. With the possibility of overestimating or underestimating the exposure ages, we attempted to solve Eq. 4 without an initial inventory correction. Regarding our NO_3^- measurements, we assumed that aside from solubilization and salt translocation, NO_3^- is preserved in the soils and any volatilization or photolysis is negligible (Diaz et al., 2020; Jackson et al., 2016).

S2. Relative exposure age calculations and estimates

S2.1 "Measured" exposure ages from Roberts Massif, Bennett Platform, and Thanksgiving Valley

We calculated exposure ages for the samples furthest from the glacier for Roberts Massif, Bennett Platform, and Thanksgiving Valley using Eq. 4, both with and without the erosion term (Table S3). The exposure ages with erosion range from 120 ka to 4.15 Ma, and the ages without erosion range from 110 ka to 1.67 Ma for Bennett Platform and Roberts Massif, respectively. Thanksgiving Valley is intermediate with an exposure age of 540 ka with erosion and 500 ka without erosion. Since we are not able to correct for initial inventory or inheritance, the exposure ages with the erosion term represent maximum ages. The erosion rate we estimated is relatively low compared to the calculated exposure ages for most samples and would only slightly influence the measured exposure ages. Roberts Massif is an exception where the inclusion or exclusion of erosion alters the measured age by over 50%. Moreover, the ages without erosion terms are probably overestimates as well without inheritance corrections.

S2.2 "Estimated" exposure ages using inventory relationship

The concentration patterns of NO_3^- and ^{10}Be at depth are parallel or mirrored (e.g., Bennett Platform), and we further evaluate their relationship. When plotted on log scales, NO_3^- and ^{10}Be have a strong power-law relationship (selected to accommodate scale differences) with R^2 values ranging from 0.66 to 0.99 (Fig. S1). Bennett Platform has the only non-significant relationship, with a p-value greater than 0.05 (p-value = 0.39). The regression slopes for Roberts Massif and Thanksgiving Valley are positive, while Bennett Platform has a negative slope where increasing ^{10}Be concentrations correlate with decreasing NO_3^- concentrations. Given these regressions, we attempt to estimate ^{10}Be concentrations using NO_3^- concentrations, and ultimately calculate "estimated" inventories and surface exposure ages using Eqs. 2 and 4 for these three locations.

The estimated inventories (using the NO_3^- regression) with erosion range from 0.14 x 10^{11} atoms at Bennett Platform to 1.5 x 10^{11} atoms at Roberts Massif (Table S4). The measured (see Section 5.1) and estimated inventories differ by ~3-18%. The "estimated" exposure ages using the estimated inventory range from 120 ka to 4.5 Ma with erosion, and the ages without erosion range from 110 ka to 1.7 Ma for Bennett Platform and Roberts Massif, respectively (Table S3). The estimated ages for Thanksgiving Valley are ~430 ka and 390 ka with and without erosion, respectively. The measured and estimated exposure ages only differ by ~4-20% for Roberts Massif, Bennett Platform, and Thanksgiving Valley. We acknowledge the complexity of this environment with and attempt to apply this simple method to the other locations with NO_3^- depth profiles.

Applying the regression from Thanksgiving Valley to Mt. Augustana, Mt. Franke and Mt. Heekin, and the regression from Roberts Massif to Schroeder Hill, we provide estimates of meteoric ^{10}Be concentrations for the entire depth profiles (Table S4) and use these concentrations to calculate an estimated inventory using Eq. 2. The inventories range from 1.1 x 10^{11} atoms at Schroeder Hill to 0.27 x 10^{11} atoms at Mt. Franke (Table S3). Further, the estimated inventories are used to estimate exposure ages using Eq. 4, both with and without the erosion term, as described above. Since we cannot calculate exposure ages using only ^{10}Be for the profiles from Schroeder Hill, Mt. Augustana, Mt. Heekin, and Mt. Franke, we are not able to compare the estimated ages with the ones calculated using ^{10}Be alone (measured ages). Instead, we can compare the estimated surface ^{10}Be concentrations using NO_3^- to the actual ^{10}Be concentrations. The percent differences at Schroeder Hill and Mt. Heekin are low 4% and 7%, respectively, while Mt. Augustana and Mt. Franke have higher differences of 36% and 40%, respectively (Tables S3; S4).

We show that the differences between measured ^{10}Be inventories and estimated inventories using NO_3^- are low and argue that the regressions between meteoric ^{10}Be and NO_3^- can be used to expand our current exposure age database for the TAM; compared to cosmogenic radionuclide analyses, NO_3^- analyses are rapid and cost effective. However, a model using NO_3^- or salts alone is likely insufficient to precisely determine an age, unless the anion accumulation rates, removal mechanisms, and mobility in soil are constrained (Graham et al., 2002; Schiller et al., 2009). Though the regressions between NO_3^- and ^{10}Be are strong (Fig. 6c), each of the three profiles from Roberts Massif, Bennett Platform, and Thanksgiving Valley have different regression coefficients and slopes. In other words, the nature of the relationship between meteoric ^{10}Be and NO_3^- varies across the Shackleton Glacier region and varies depending on the location. This was expected given the complex history of ice cover, exposure, disturbance, and wetting for soils across the Shackleton Glacier region. To address some of these uncertainties, ^{10}Be data (surface samples for all locations and a few depth profiles) are necessary to constrain the most accurate regression and minimize the associated error.

We tested our meteoric $^{10}Be - NO_3^-$ model with data from Arena Valley in the MDV (Graham et al., 2002) and found that our model can be applicable for other TAM ice-free areas. Similar to most Shackleton Glacier region soils, the soils from Arena Valley are hyper-arid with high concentrations of NO_3^- and other salts (Graham et al., 2002). Precipitation in the MDV is low at ~5 cm water equivalent each year (Fountain et al., 1999), though NO_3^- and other water-soluble salts at the surface can be wetted and mobilized. The highest NO_3^- concentrations are at 10 cm depth, while ^{10}Be concentrations are highest at the surface and decrease with depth, indicating vertical transport of NO_3^- through time (Graham et al., 2002). The regression between ^{10}Be and NO_3^- throughout the profile is weaker for the Arena Valley samples compared to Shackleton Glacier samples; there is a stronger correlation in the top 20 cm ($R^2 = 0.61$) compared to the bottom 70 cm ($R^2 < 0.01$) and the profile is considerably deeper (110 cm). Using the regression from Bennett Platform, which mostly closely resembles the profile behavior for Arena Valley given the negative slope, the estimated inventory is 5.4×10^{10} atoms. The measured inventory is of the same order of magnitude, 1.3×10^{10} atoms, indicating a moderate model fit. Using the regression from the from Arena Valley samples, the estimated inventory is 9.2×10^{9} atoms, which is ~27% lower than the measured inventory. These results indicate that, although the Shackleton Glacier region is nearly 900 km from Arena Valley, the correlation between NO_3^- and meteoric ^{10}Be might be applicable in other hyper-arid Antarctic soils. However, as stated previously, NO_3^- and meteoric ^{10}Be data are needed to ascertain the general profile and slope behavior within the region, and a general knowledge of the exposure history of the region can help constrain ages (Everett, 1971). This $^{10}Be - NO_3^-$ dating tool will need to be further evaluated with additional measurements and erosion, initial inventory, and inheritance corrections.

S3. Measured, estimated, and inferred exposure age validation

Considering the novelty of our approach, we sought to test and externally validate our exposure ages. Our measured, inferred, and estimated exposure ages are consistent with the limited *in-situ* exposure age data from the Shackleton Glacier region (http://antarctica.ice-d.org; Balco, 2020). Exposure ages from glacial erratic boulders using *in-situ* cosmogenic measurements were determined in previous studies (Balter-Kennedy et al., 2020; Balco, 2020; http://antarctica.ice-d.org) from Roberts Massif, Thanksgiving Valley, and Mt. Franke (Figs. S2; S3). From *in-situ* ^{10}Be, ^{26}Al, ^{3}He, and ^{21}Ne data, exposure ages on the northern flank of Roberts Massif range from 1.10 Ma to 3.26 Ma (Balter-Kennedy et al., 2020; Balco, 2020; http://antarctica.ice-d.org), and our measured, inferred, and estimated ages without erosion are 1.67 Ma, 1.94 Ma, and 1.74 Ma, respectively. Our ages, which are likely overestimates due to a lack of initial inventory or inheritance corrections, are comparable to these nearby *in-situ* ages at similar elevations (Figs. S2; S3). The ages with the erosion term are greater and outside the range from Balter-Kennedy et al. (2020). This indicates that either soil erosion rates are low at Roberts Massif, and/or the initial inventory and ^{10}Be inheritance from previous exposures are likely significantly smaller than the measured inventory. Otherwise, the inheritance-corrected exposure ages would be much greater than the *in-situ* ages.

To the north, the *in-situ* ages from erratic boulders at Thanksgiving Valley vary greatly from ~4.3 ka near the glacier to 450 ka at higher elevations, though most ages appear to be around 30 ka (Figs. S2; S3) (Balco, 2020; http://antarctica.ice-d.org). Our exposure ages are greater than most previous ages. In particular, the sample collected closest to Shackleton Glacier has an inferred age two orders of magnitude higher than the *in-situ* age from a nearby glacial erratic at the same elevation (Fig. S4), though this could be reflective of a relatively large ^{10}Be inheritance. Given the location (~100 m from the glacier) and young nearby *in-situ* age (~4.3 ka), this location was likely covered during the LGM and other glacial periods.

Closer to the Ross Ice Shelf, the *in-situ* ages from Mt. Franke range from ~29 ka to 220 ka. Our estimated age without erosion is at the top that range at 220 ka, though the inferred ages are considerable younger at 94 ka and 72 ka (Table 3). Similar to Roberts Massif, our ages from Mt. Franke ages are comparable to the *in-situ* ages from similar elevations (Fig. S4). Here, soil erosion, initial inventory, and inheritance may minimally influence the measured ^{10}Be inventory. We argue that while the measured, inferred, and estimated ages are similar to *in-situ* ages, they are likely an overestimate and most useful from a relative perspective in understanding which surfaces have been exposed for longer than others. Additionally, sensitivity analyses need to be completed to interrogate erosion rates and regression coefficients.

While the exposure age proxies we investigated (^{10}Be inventory and ^{10}Be – NO_3^- estimation) show some initial promise, more data and analyses are needed to determine whether these methods produce accurate relative ages.

Figure S1: Relationship between meteoric ^{10}Be and NO_3^- for Roberts Massif (orange), Bennett Platform (green), and Thanksgiving Valley (blue). Each site is fit by a power-law function and R^2 values for the regressions are shown. These regressions are used to estimate concentrations of ^{10}Be to estimate exposure ages.

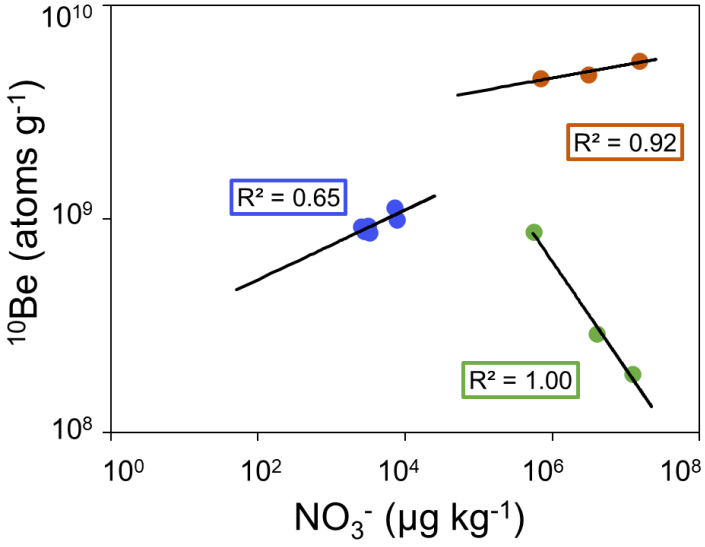

Figure S2: *In-situ* exposure age measurements from glacial erratic boulders (brown filled triangles) (http://antarctica.ice-d.org; Balco, 2020; Balter-Kennedy et al., 2020) in relation to the meteoric ^{10}Be sample locations from Roberts Massif (a, orange outline), Thanksgiving Valley (b, blue outline), and Mt. Franke (c, grey outline). Pleistocene-age moraines described by Balter-Kennedy et al. (2020) are labeled at Roberts Massif in green. We identified moraines (green) of an unknown age at Mt. Franke. Base maps were provided by the Polar Geospatial Center.

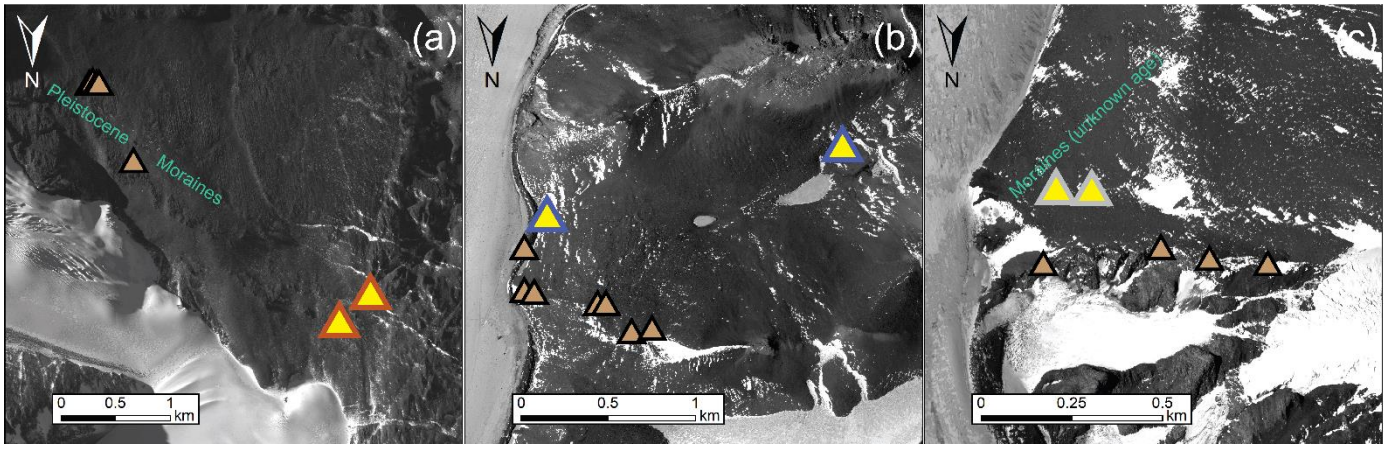

Figure S3: Estimated (using $^{10}Be - NO_3^-$ regressions) meteoric ^{10}Be exposure ages (open colored triangles) and inferred (using maximum ^{10}Be concentration) exposure ages (closed colored triangles) without erosion compared to *in-situ* ages from ICE-D (Balco, 2020) and Balter-Kennedy et al. (2020) (solid triangles) against elevation. All *in-situ* ages were measured from glacial erratic boulders.

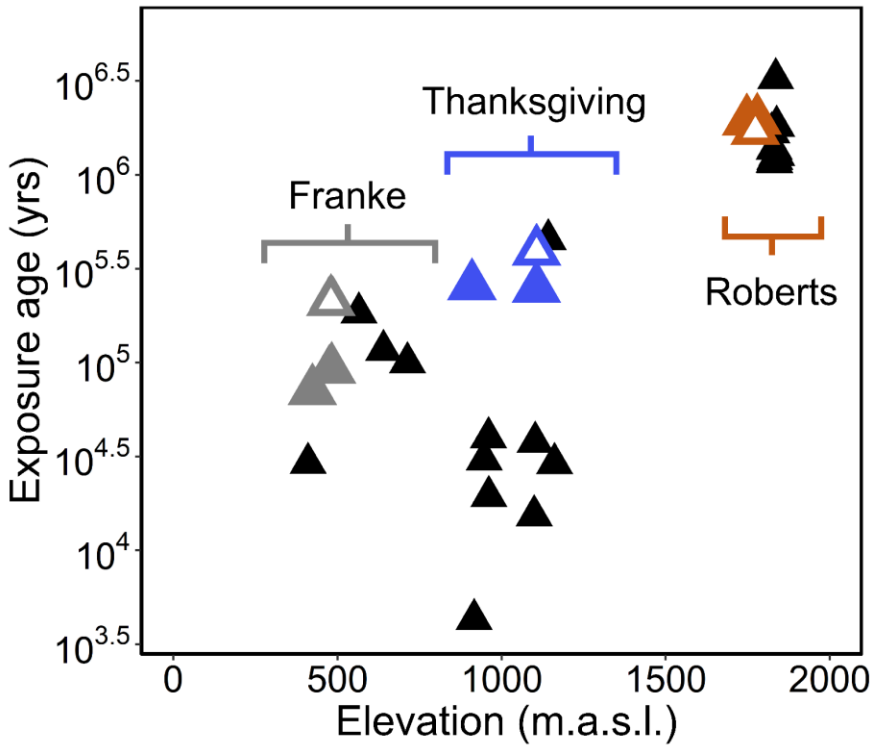

Figure S4: Inferred surface exposure ages versus distance from the coast (a) and elevation (b), with (black) and without (blue) an assumed erosion term (re-created from Fig. 8). Upward facing triangles are samples collected furthest from the glacier, while downward triangles are samples collected closest to the glacier. The estimated surface exposure ages (using $^{10}Be - NO_3^-$ regressions) are included in panel (c). Values with asterisks (*) are ages determined using the measured meteoric ^{10}Be concentrations in the depth profiles.

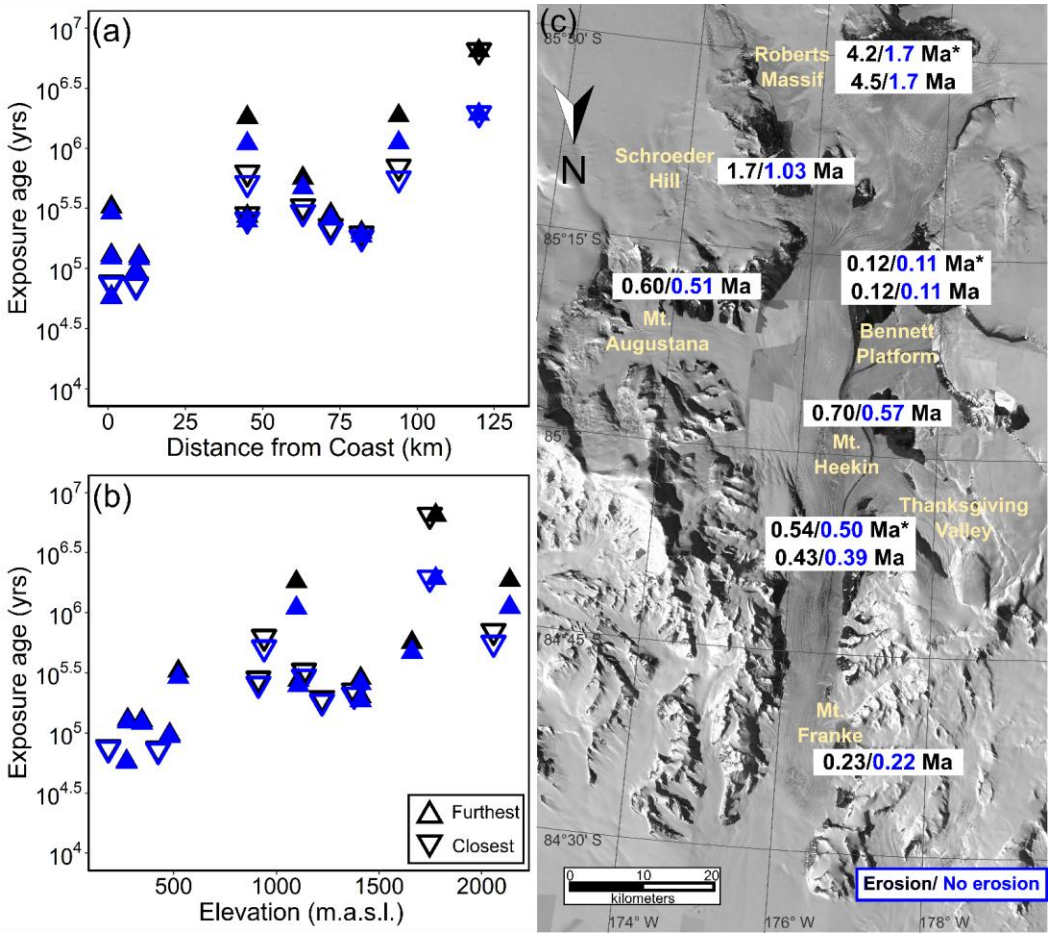

Table S1: Soil grain size distribution of surface samples and depth profiles from Roberts Massif, Bennett Platform, and Thanksgiving Valley.

Sample Name	% Gravel (>2 mm)	% Sand (63µm-2mm)	% Silt (<63 µm)
AV2-1	15.0	80.5	4.5
AV2-8	11.1	87.9	1.0
BP2-1, 0-5	34.0	61.4	4.6
BP2-1, 5-10	33.6	54.5	11.9
BP2-1, 10-15	37.8	46.2	16.0
BP2-8	15.6	83.2	1.1
MF2-1	32.1	65.8	2.1
MF2-4	34.4	64.8	0.8
MH2-1	36.0	62.0	2.1
MH2-8	31.6	67.3	1.1
MSP2-1	64.7	35.2	0.1
MSP2-4	33.6	66.1	0.3
MSP4-1	37.4	61.2	1.4
MW4-1	27.8	67.3	4.9
NP2-5	56.4	38.3	5.3
RM2-1, 0-5	13.2	69.3	17.5
RM2-1, 5-10	8.0	84.4	7.5
RM2-1, 10-15	7.5	80.8	11.7
RM2-8	24.9	68.5	6.7
SH3-2	15.7	77.3	7.0
SH3-8	4.7	92.2	3.2
TGV2-1, 0-5	27.7	71.6	0.7
TGV2-1, 5-10	32.4	66.7	0.9
TGV2-1, 10-15	44.1	54.7	1.2
TGV2-1, 15-20	29.3	69.3	1.4
TGV2-1, 20-25	21.6	76.8	1.6
TGV2-1, 25-30	52.2	45.1	2.7
TGV2-8	21.2	78.6	0.2
TN3-1	32.4	64.7	2.8
TN3-5	52.6	42.4	5.0

Table S2: Concentration of meteoric ^{10}Be in Shackleton Glacier region surface soils and depth profiles from Roberts Massif, Bennett Platform, and Thanksgiving Valley.

Sample name	Sample mass (g)	Mass of ^{9}Be added (µg)*	AMS Cathode Number	Uncorrected $^{10}Be/^{9}Be$ ratio (10^{-11})**	Uncorrected $^{10}Be/^{9}Be$ ratio uncertainty (10^{-13})**	Background-corrected $^{10}Be/^{9}Be$ ratio (10^{-11})***	Background-corrected $^{10}Be/^{9}Be$ ratio uncertainty (10^{-13})***	^{10}Be concentration (10^{9} atoms g^{-1})	^{10}Be concentration uncertainty (10^{7} atoms g^{-1})
AV2-1	0.499	394.3	151135	2.201	1.143	2.201	1.143	1.162	0.604
AV2-8	0.500	400.2	151137	1.786	1.067	1.785	1.067	0.955	0.571
BP2-1, 0-5	0.499	401.2	151147	1.616	1.055	1.615	1.055	0.868	0.567
BP2-1, 5-10	0.499	399.2	151148	0.353	0.748	0.352	0.748	0.188	0.400
BP2-1, 10-15	0.496	400.2	151149	1.573	1.894	1.573	1.894	0.848	1.021
BP2-8	0.498	400.2	151550	0.542	0.448	0.541	0.448	0.291	0.241
MF2-1	0.505	398.2	151554	3.713	3.444	3.712	3.444	1.956	1.815
MF2-4	0.501	398.2	151555	2.448	1.395	2.447	1.396	1.300	0.741
MH2-1	0.498	399.2	151138	0.864	0.820	0.863	0.820	0.462	0.439
MH2-8	0.499	395.3	151139	0.681	0.847	0.680	0.847	0.360	0.449
MSP2-1	0.499	403.2	151556	0.539	0.464	0.538	0.464	0.291	0.250
MSP2-4	0.502	402.2	151557	0.693	0.673	0.692	0.674	0.370	0.361
MSP4-1	0.499	400.2	151566	1.112	1.117	1.111	1.117	0.596	0.598
MW4-1	0.498	400.2	151564	1.093	0.662	1.092	0.662	0.586	0.356
NP2-5	0.496	402.2	151565	2.391	1.200	2.391	1.200	1.295	0.650
RM2-1, 0-5	0.502	399.2	151558	8.541	4.116	8.541	4.116	4.538	2.187
RM2-1, 5-10	0.499	398.2	151559	8.853	8.411	8.852	8.411	4.721	4.485
RM2-1, 10-15	0.500	400.2	151560	13.70	8.460	13.70	8.460	7.327	4.524
RM2-8	0.498	401.2	151561	10.17	15.27	10.17	15.27	5.475	8.221
SH3-2	0.497	398.2	151551	7.191	3.129	7.190	3.129	3.850	1.675
SH3-8	0.501	398.2	151552	4.270	3.351	4.269	3.351	2.267	1.780
TGV2-1, 0-5	0.498	398.2	151140	1.860	2.431	1.859	2.431	0.993	1.299
TGV2-1, 5-10	0.500	398.2	151141	1.731	1.589	1.731	1.589	0.921	0.846
TGV2-1, 10-15	0.497	393.3	151142	1.635	1.377	1.634	1.377	0.864	0.728

TGV2-1, 15-20	0.502	399.2	151143	1.645	1.776	1.645	1.777	0.874	0.944
TGV2-1, 20-25	0.498	403.2	151144	1.711	0.852	1.710	0.852	0.925	0.461
TGV2-1, 25-30	0.497	399.2	151145	2.148	2.071	2.147	2.071	1.152	1.112
TGV2-8	0.499	399.2	151146	2.106	2.185	2.105	2.185	1.125	1.168
TN3-1	0.500	401.2	151562	7.092	5.903	7.091	5.903	3.802	3.165
TN3-5	0.500	401.2	151563	3.926	5.694	3.925	5.694	2.105	3.053
*^{9}Be was added through commercial SPEX carrier with a concentration of 1000 µg mL^{-1}.									
**Isotopic analysis was conducted at PRIME Laboratory; ratios were normalized against standard 07KNSTD3110 with an assumed ratio of 2850 x 10^{-15} (Nishiizumi et al., 2007). Blank ^{10}Be/^{9}Be ratio values averaged 8.152 ± 1.884 x 10^{-15}.									

Table S3: Exposure ages calculated from Eq. (1-4) and estimated ages using $^{10}Be - NO_3^-$ regressions (Fig. S1).

Location	**Measured inventory (10^{11} atoms)**	**Measured exposure age with *E* (Ma)**	**Measured exposure age without *E* (Ma)**	**Estimated inventory (10^{11} atoms)***	**Estimated exposure age with *E* (Ma)***	**Estimated exposure age without *E* (Ma)***
Augustana	-	-	-	0.580	0.601	0.505
Bennett	0.135	0.115	0.106	0.143	0.122	0.113
Franke	-	-	-	0.268	0.232	0.217
Heekin	-	-	-	0.646	0.703	0.571
Roberts	1.47	4.15	1.67	1.51	4.54	1.74
Schroeder	-	-	-	1.05	1.66	1.03
Thanksgiving	0.570	0.535	0.495	0.465	0.426	0.394
*Estimations derived from linear relationship between NO3- concentration and meteoric 10Be concentration						

Table S4: NO_3^- concentrations and estimate of ^{10}Be concentration from linear relationship between NO_3^- and ^{10}Be.

Location	Depth (cm)	NO_3^- (10^5 µg kg^{-1})	^{10}Be estimate (10^9 atoms g^{-1})
Augustana	0	7.77	1.83
Augustana	5	12.2	1.97
Augustana	10	13.4	2.00
Schroeder	0	75.5	3.70
Schroeder	5	16.1	3.26
Schroeder	10	41.6	3.52
Franke	0	0.041	0.78
Franke	5	0.014	0.65
Franke	10	0.010	0.62
Franke	15	0.011	0.63
Roberts	0	6.94	4.57
Roberts	5	149	5.52
Roberts	10	30.7	5.01
Bennett	0	5.57	0.90
Bennett	5	39.8	0.34
Bennett	10	121	0.19
Thanksgiving	0	0.077	0.86
Thanksgiving	5	0.071	0.85
Thanksgiving	10	0.025	0.72
Thanksgiving	15	0.033	0.75
Thanksgiving	20	0.028	0.73
Thanksgiving	25	0.031	0.74
Heekin	0	18.0	2.10
Heekin	5	27.4	2.25
Heekin	10	18.8	2.11